Electrodeposited Polyoxometalate-$Cu_{2+1}O$ Hybrid on Copper Foam: Synergistic Electron Transfer for Efficient Nitrate Electroreduction to Ammonia

Kaiqun Bai, Xinming Wang*, Gang Li, Haijun Pang, and Huiyuan Ma

a School of Materials Science and Chemical Engineering, Harbin University of Science and Technology, Harbin 150040, PR China.

*Correspondence: wangxinming20@126.com (X. M. Wang).

Text S1

Chemicals and materials.

Amonium molybdate tetrahydrate ($H_{32}Mo_7N_6O_{28}$) (Mo_7), Copper sulfate pentahydrate ($CuSO_4 \cdot 5H_2O$), sulphuric acid (H_2SO_4), Copper foam (12 mm × 12 cm × 12 cm) were purchased from Saibo Chemical Reagents Co., Ltd. All commercial chemicals were used without further purification unless otherwise mentioned.

Characterizations.

High-resolution transmission electron microscopy (HRTEM) images and elemental mapping were performed on a JEOL JEM-2200FS operating at 200 kV. Scanning electron microscopy (SEM) images were performed on a Zeiss Supra55. Fourier transform infrared (FT-IR) spectra were collected on a Bruker Vector 22 infrared spectrometer using the KBr pellet method at wavenumbers ranging from 4000 to 400 cm^{-1}. X-ray diffraction (XRD) patterns were collected by a Rigaku XRD-6000 diffractometer equipped with a Cu Kα radiation (λ = 1.5405 Å). N_2 adsorption-desorption measurements were determined on a Micromeritics ASAP 2020 M surface area and porosity analyzer, with samples pre-degassing under vacuum at 100 ^oC for 6 h. X-ray photoelectron spectroscopy (XPS) spectra were performed on a monochromatized ALK exciting X-radiation (PHI Quantera SXM), which were calibrated against C 1s at 284.8 eV. Gas chromatography (GC) was quantitatively analyzed using an HF-901A gas chromatograph (China Huifen) with flame ionization detector (FID). UV-visible spectra were measured on a U-3900 UV-vis spectrophotometer (Hitachi, Japan). All the electrochemical tests were carried out in a three-electrode testing system (CHI 760E electrochemical workstation, Chenhua, Shanghai). A conventional three-electrode system was used, using the prepared catalyst material as the working electrode, a commercial Ag/AgCl as reference electrode and a Pt wire as counter electrode. ^1H nuclear magnetic resonance (NMR) experiments were carried out at 303 K for 5 % w/v sample solution in DMSO-d_6 using Bruker Avance NEO 300. The in-situ attenuated total reflection Fourier-transformed infrared spectroscopy (ATR-FTIR) uses the Nicolet iS20 (Thermo Fisher Scientific, USA) and photoelectrochemistry in-situ attenuated total reflection infrared reaction cell (EC-

ATR-H, Beijing Scistar Technology Co. Ltd.)

Text S2

Preparation of the Modified Electrodes.

The fabricated electrodes were subsequently soaked in acetone to remove residual electrodeposited layers and then dried.

Mo_7@TBAB: Given the poor intrinsic electrical conductivity of POMs, acetylene black (AB) was introduced to mix with the as-synthesized POMs to improve the conductivity. Nafion solution was introduced as a kind of POMs dispersion solution generally applied in many reported works, which can form a homogeneous ink with POMs and further help to attach onto the surface of carbon cloth. The preparation of the CCE working electrode was as follows. A volume of 0.15 mg electrocatalyst, 0.15 mg acetylene black (AB), 365 μL deionized water, 125 μL isopropyl alcohol and 10 μL Nafion solution (0.1 wt% water solution) are grounded to form uniform catalyst ink. After sonication for 30 min, the ink was dropped directly onto a carbon cloth (1 cm × 1 cm) with a catalyst loading density of ~0.03 mg cm^{-2} and dried.

Electrochemical Measurements.

NO_3RR experiments were performed in a typical H-cell arrangement separated by a Nafion 211 membrane at room temperature. Before NO_3RR test, Nafion membrane was protonated by first boiling in water for 1 h, then in H_2O_2 for 1 h, then in water for another hour, followed by 3 h in 0.5 M H_2SO_4, and finally for 6 h in water. All steps were performed at 80 °C. The electrochemical measurements were conducted by a CHI 760 electrochemical analyzer (Shanghai, Chenhua Co., China) in a three-electrode cell containing electrolyte. The potentials reported in this work were converted to RHE scalevia calibration with the following equation: E (vs. RHE) = E (vs. Ag/AgCl) + 0.197 + 0.059 × pH, and the polarization curves were the steady-state ones after several cycles. The presented current density referred to the geometrical area of the CC.

Product quantification

Ammonia: 2 mL electrolyte was removed from the cathodic chamber and mixed with oxidizing solution containing 2 mL NaOH solution (1.0 M) containing salicylic acid (5 wt %), sodium citrate (5 wt %), 1 mL of NaClO (0.05 M), and 0.2 mL of 1 wt % $Na_2[Fe(NO)(CN)_5]$ for 2 h. The solution was measured with UV–vis absorption

spectrum at 652 nm. Calibration curve of NH_3 in electrolyte solution was plotted using a series of different concentration of standard ammonia stock solution diluted by 0.1 M HCl.

Nitrite: to prepare the color reagent, phosphoric acid (1 mL, ρ=1.70 g/mL), N-(1-Naphthyl) ethylenediamine dihydrochloride (0.02 g) and p-aminobenzene sulfonamide (0.4 g) were dissolved in deionized water (5 mL). the collected electrolyte was diluted several times and the pH was adjusted by phosphoric acid. Subsequently, the color reagent (0.1 mL) and the diluted electrolyte (5 mL) were mixed for 20 min. The absorption spectrum was obtained by UV-vis spectrophotometry at a wavelength of 540 nm.

H_2: Firstly, 300 μL gas was taken out from the electrolytic cell and injected into the gas chromatography (GC-9800). Then the peak areas of H_2 were recorded. The production of the hydrogen curve was calibrated using a series of standard volume H_2 of 0 mL, 0.1 mL, 0.2 mL, 0.3 mL, and 0.4 mL, respectively.

Isotope Labeling Experiments

To unequivocally confirm the nitrogen source of the produced ammonia, ^{15}N isotopic labeling experiments were performed. The procedure was identical to the standard tests, but the electrolyte was replaced with an Ar-saturated 0.1 M Na_2SO_4 solution containing 1000 ppm N of $K^{15}NO_3$. The resulting $^{15}NH_3$ and $^{14}NH_3$ products were characterized by ^1H NMR spectroscopy on a Bruker Avance-400 MHz spectrometer, using D_2O (99.9 atom% D, Aladdin) as the lock solvent.

Determination of Faradaic efficiency and ammonia yield rate

The calculation equations of electrochemical nitrate-to-ammonia reduction (ENRA) are as follows:

$$\text{Faradaic efficiency } (^{FE}_{NH_3}) = 8\ F \times (^{C}_{NH_3} \times V)/(^{M}_{NH_3} \times Q)$$

$$\text{Ammonia yield rate } (^{Yield}_{NH_3}) = (^{C}_{NH_3} \times V)/(t \times S)$$

where F is the Faraday constant (96485 $C \cdot mol^{-1}$), Q is the charge accumulated *via* 1 h electrocatalysis, and V is the volume of the 0.1 M Na_2SO_4 and 0.1 M KNO_3

electrolyte (50 mL), C_{NH_3} is the measured NH_3 concentration, M_{NH_3} is the molar mass of NH_3 (17 g/mol), t is the reduction reaction time (1 h) and $S_.$ is the working electrode area (1 cm^2).

$$\text{Faradaic efficiency } (FE_{NO_2^-}) = 2F \times (C_{NO_2^-} \times V)/(M_{NO_2^-} \times Q)$$

$$\text{Ammonia yield rate } (Yield_{NO_2^-}) = (C_{NO_2^-} \times V)/(t \times S)$$

where $C_{NO_2^-}$ is the measured NO_2^- concentration, $M_{NO_2^-}$ is the molar mass of NO_2^- (46 g/mol).

Supplementary tables and Figs

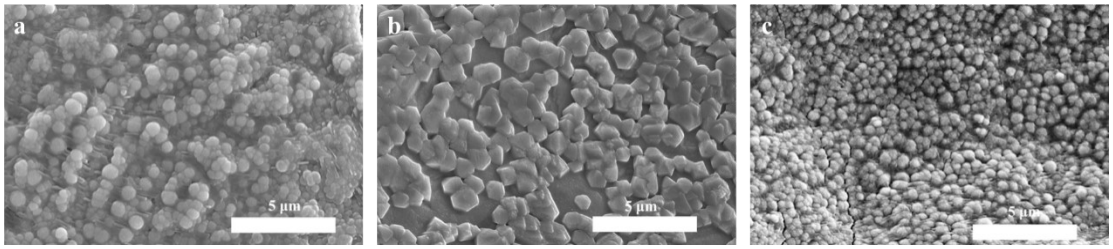

Fig. S1 SEM images of samples with different scanning rates ($mV \cdot s^{-1}$)：(a)25, (b) 50, (c) 75

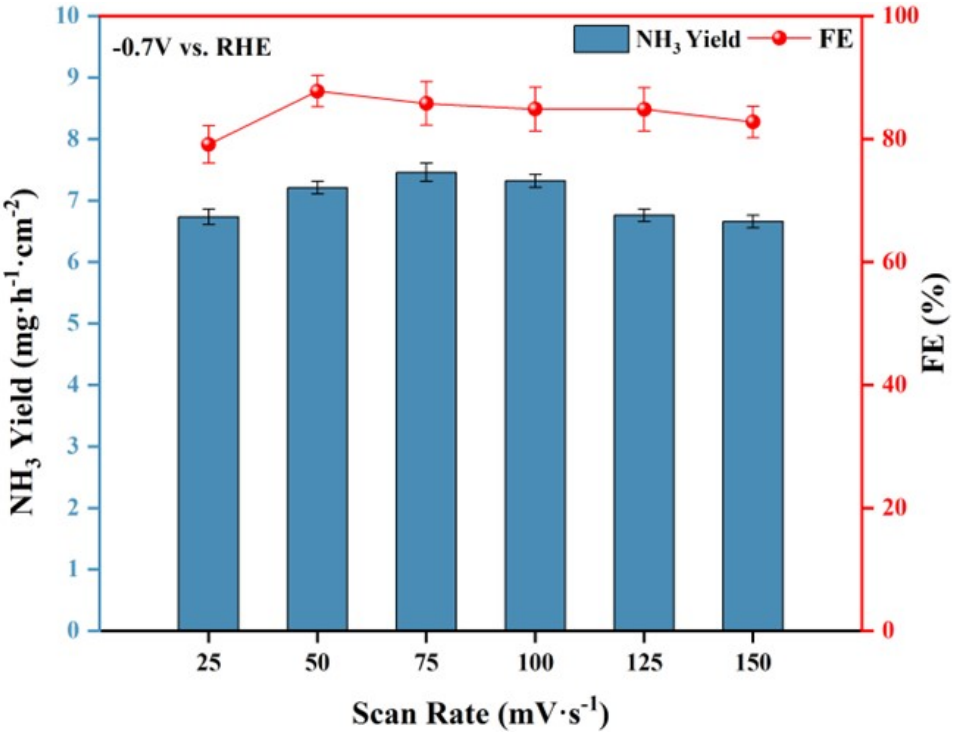

Fig. S2 NH_3 yield rates and FEs of different scanning rates $Mo_7/Cu_{2+1}O/Cu@CF$ 0.1 M Na_2SO_4 + 0.1 M KNO_3.

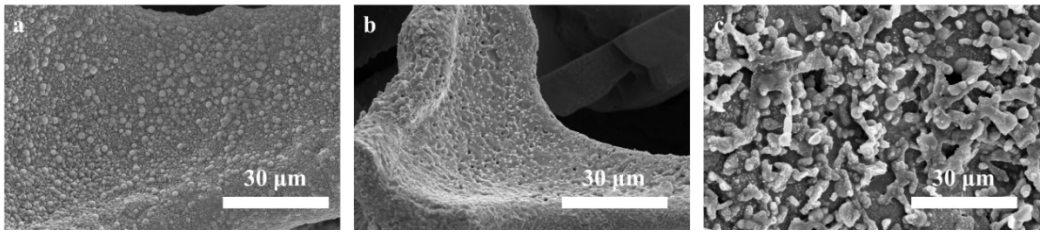

Fig. S3 SEM images of samples with different cycles;(a)1, (b)3, (c)5

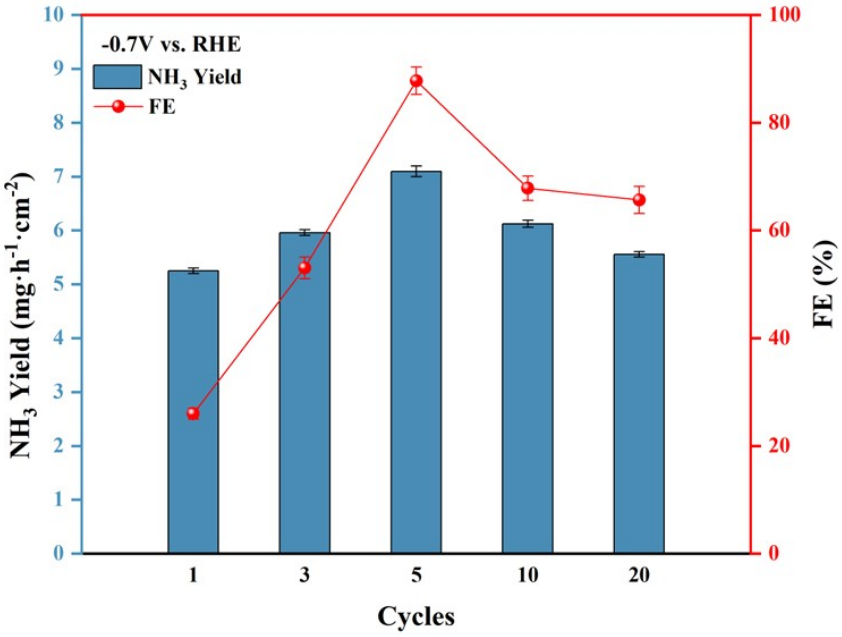

Fig. S4 NH_3 yield rates and FEs of different cycles (2 segments) $Mo_7/Cu_{2+1}O/Cu@CF$ 0.1 M Na_2SO_4 + 0.1 M KNO_3.

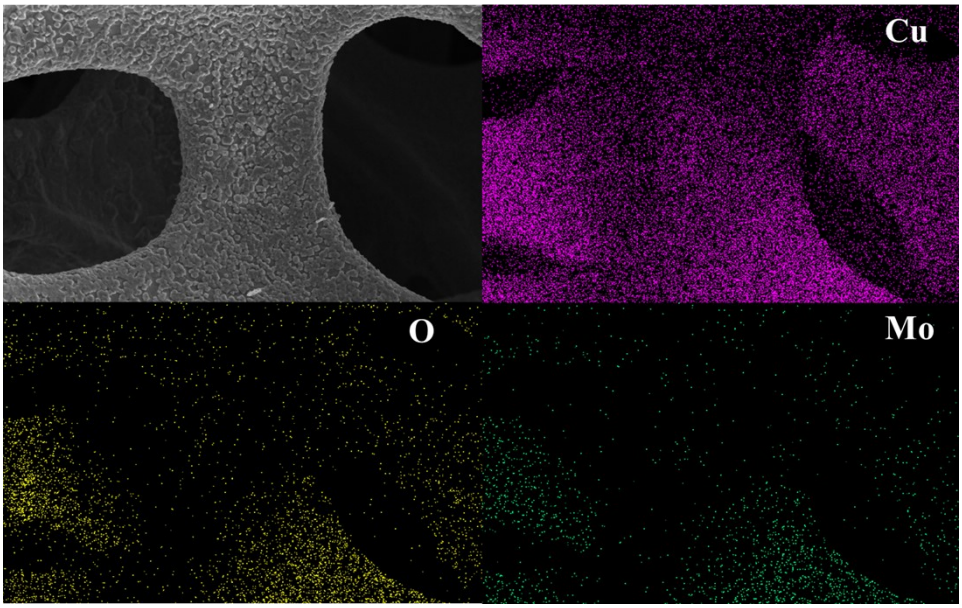

Fig. S5 SEM images and corresponding elemental mapping of $Mo_7/Cu_{2+1}O/Cu@CF$.

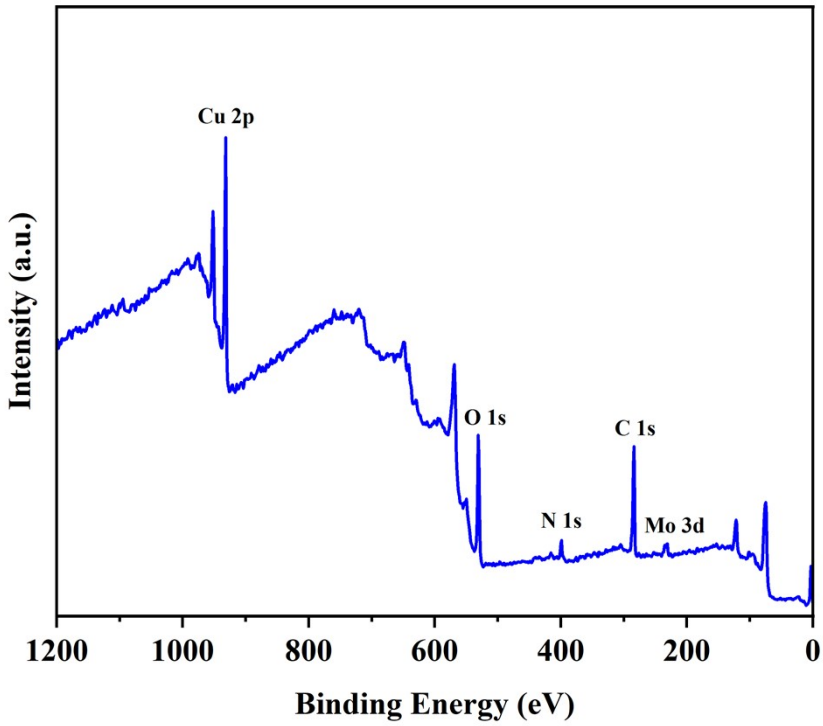

Fig. S6 XPS survey spectra of $Mo_7/Cu_{2+1}O/Cu@CF$.

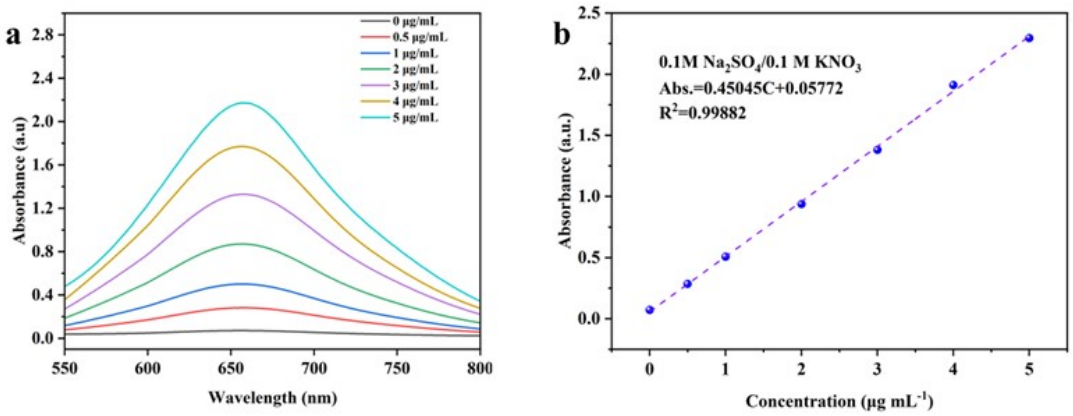

Fig. S7 (a) UV-vis absorption spectra of standard solutions with different ammonia concentrations determined by indophenol blue method. (b) The corresponding calibration curves.

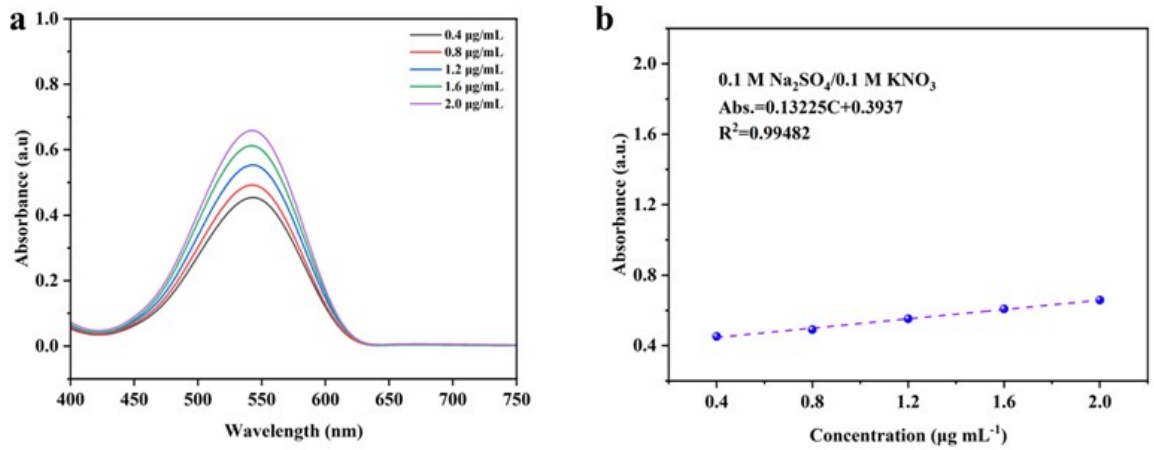

Fig. S8 (a) UV-vis spectra of NO_2^- solution with different concentrations in 0.1 M Na_2SO_4 (b) corresponding liner fitting between absorbance and NO_2^- concentration.

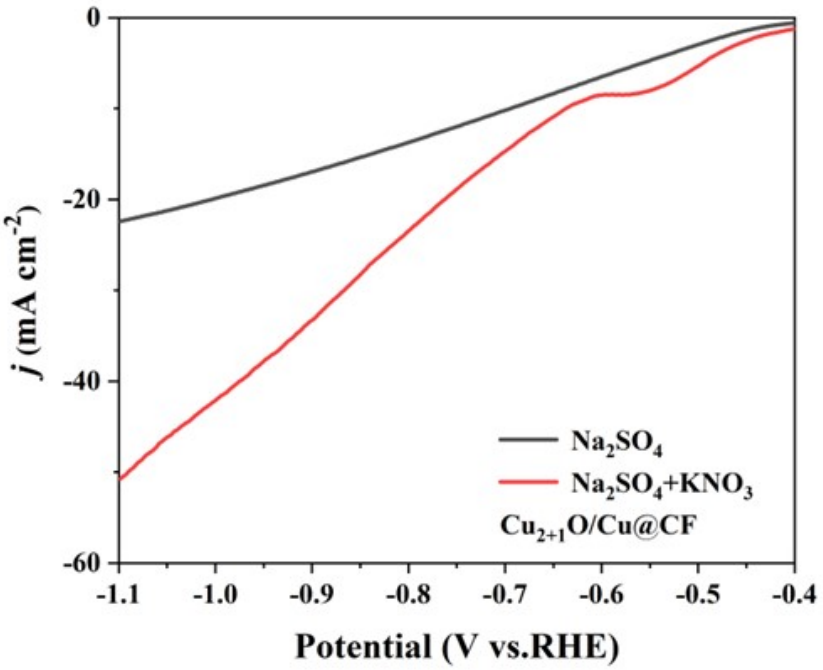

Fig. S9 LSV curves of $Cu_{2+1}O$/Cu@CF in 0.1 M Na_2SO_4 and 0.1 M Na_2SO_4 + 0.1 M KNO_3 electrolyte.

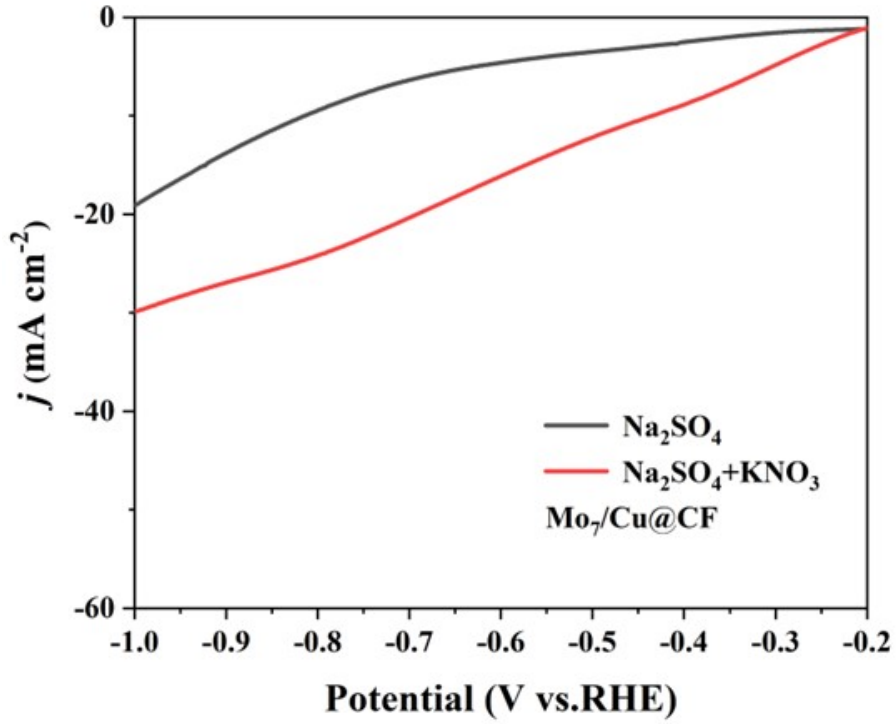

Fig. S10 LSV curves of Mo_7/Cu@CF in 0.1 M Na_2SO_4 and 0.1 M Na_2SO_4 + 0.1 M KNO_3 electrolyte.

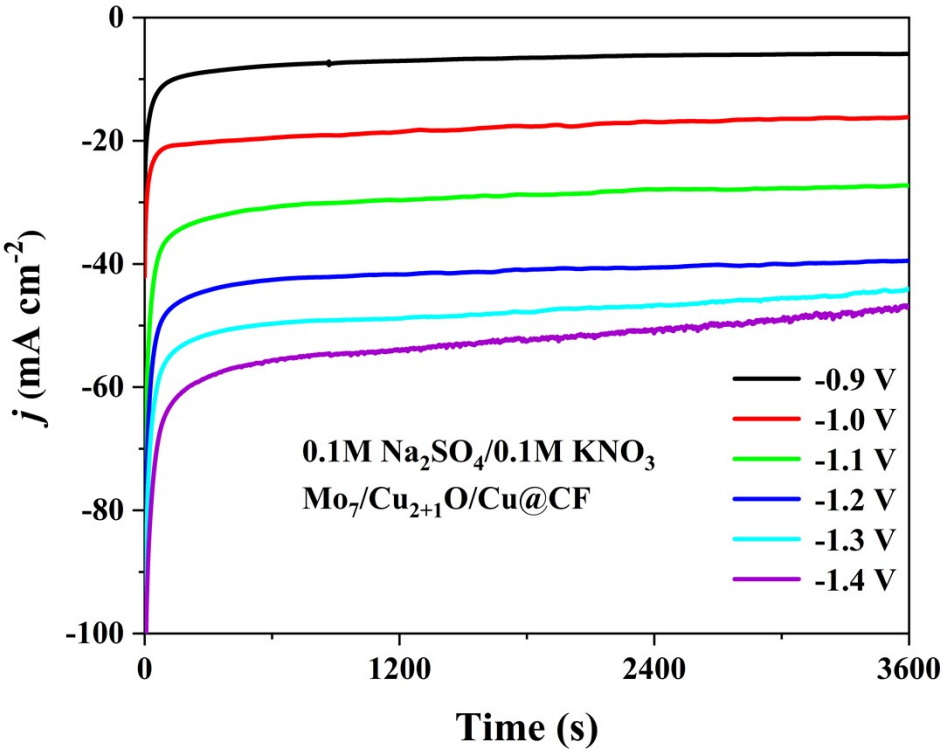

Fig. S11 Chronoamperometry test at various potentials of $Mo_7/Cu_{2+1}O$/Cu@CF.

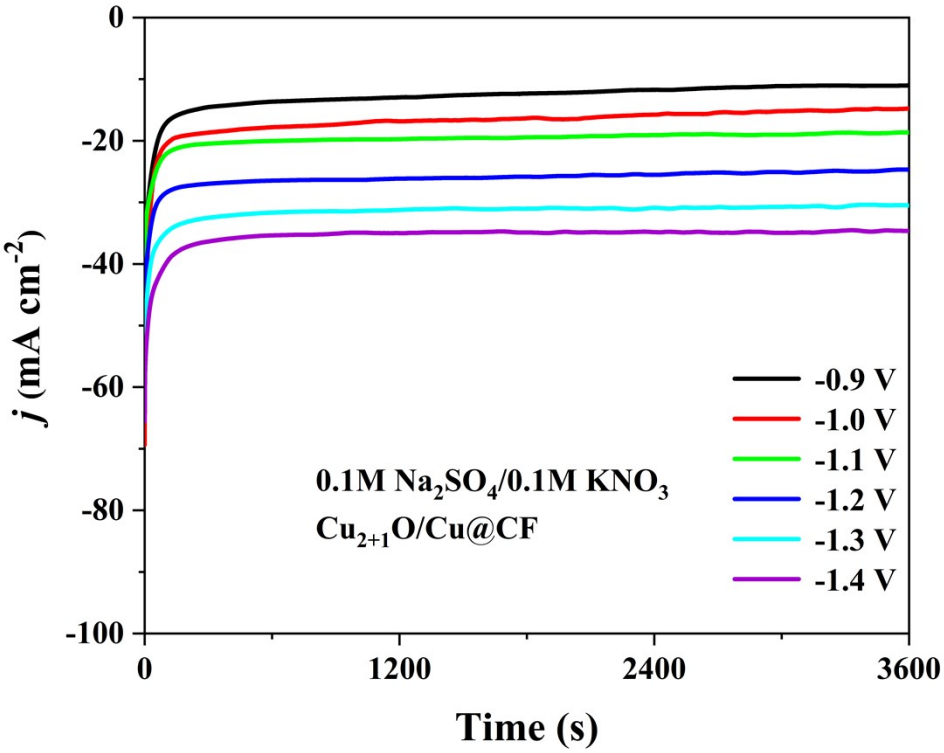

Fig. S12 Chronoamperometry test at various potentials of $Cu_{2+1}O$/Cu@CF.

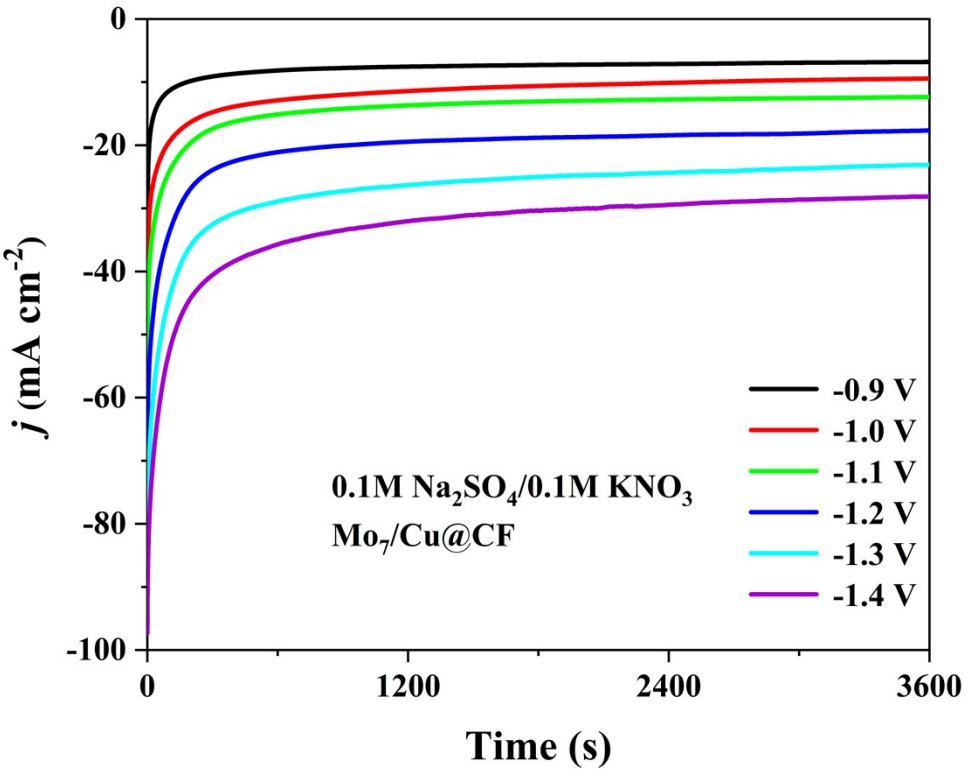

Fig. S13 Chronoamperometry test at various potentials of Mo_7/Cu@CF.

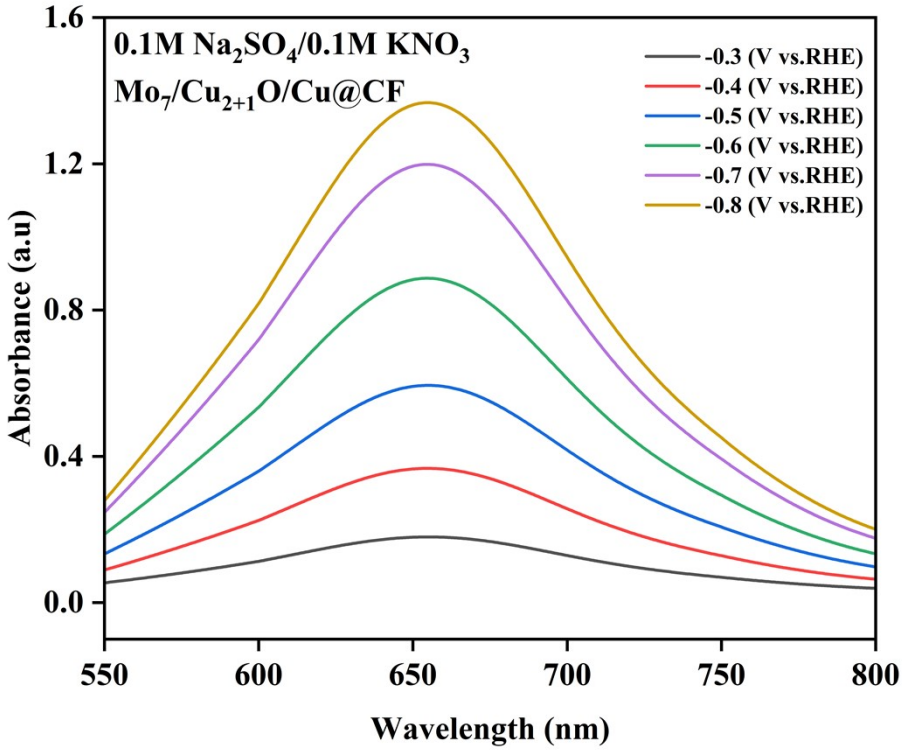

Fig. S14 UV–vis absorption spectra of $Mo_7/Cu_{2+1}O/Cu@CF$.

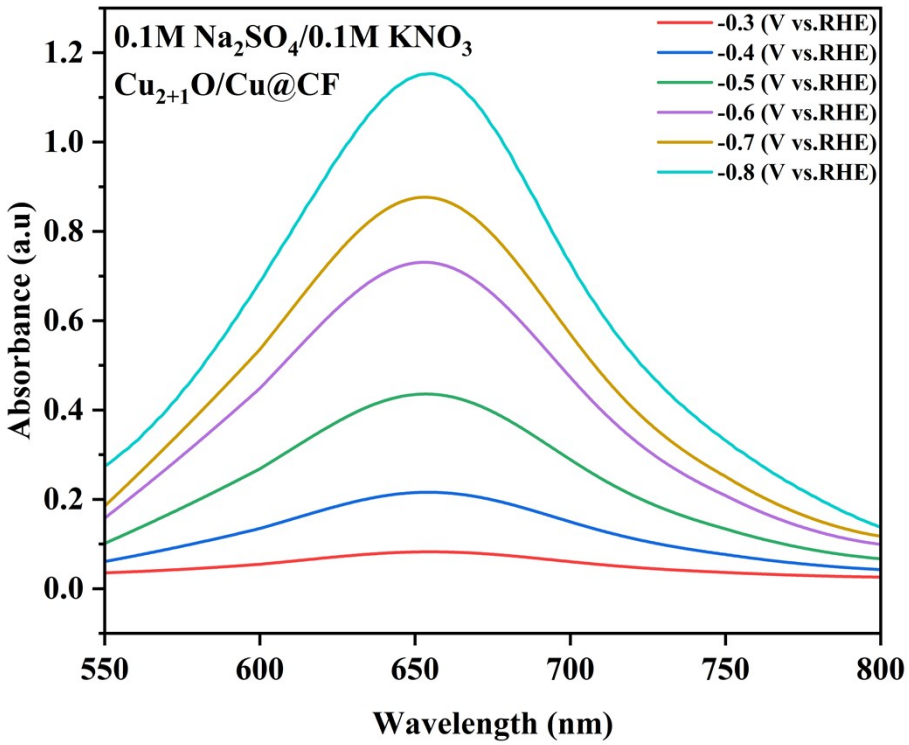

Fig. S15 UV–vis absorption spectra of $Cu_{2+1}O$/Cu@CF.

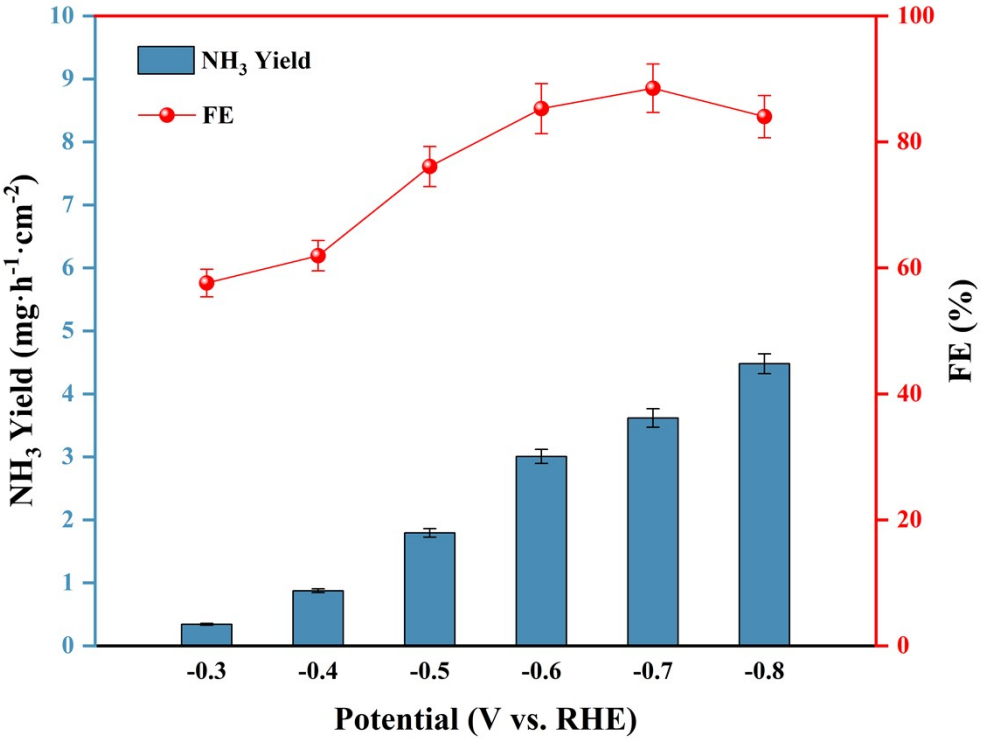

Fig. S16 NH_3 yield and FEs of $Cu_{2+1}O$/Cu@CF.

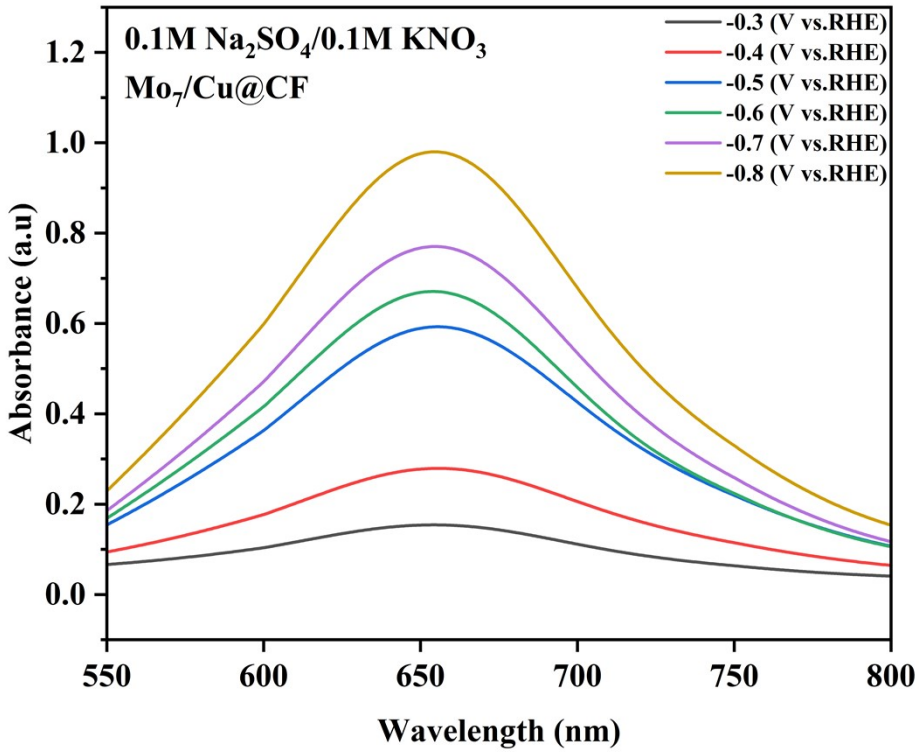

Fig. S17 UV–vis absorption spectra of Mo_7/Cu@CF.

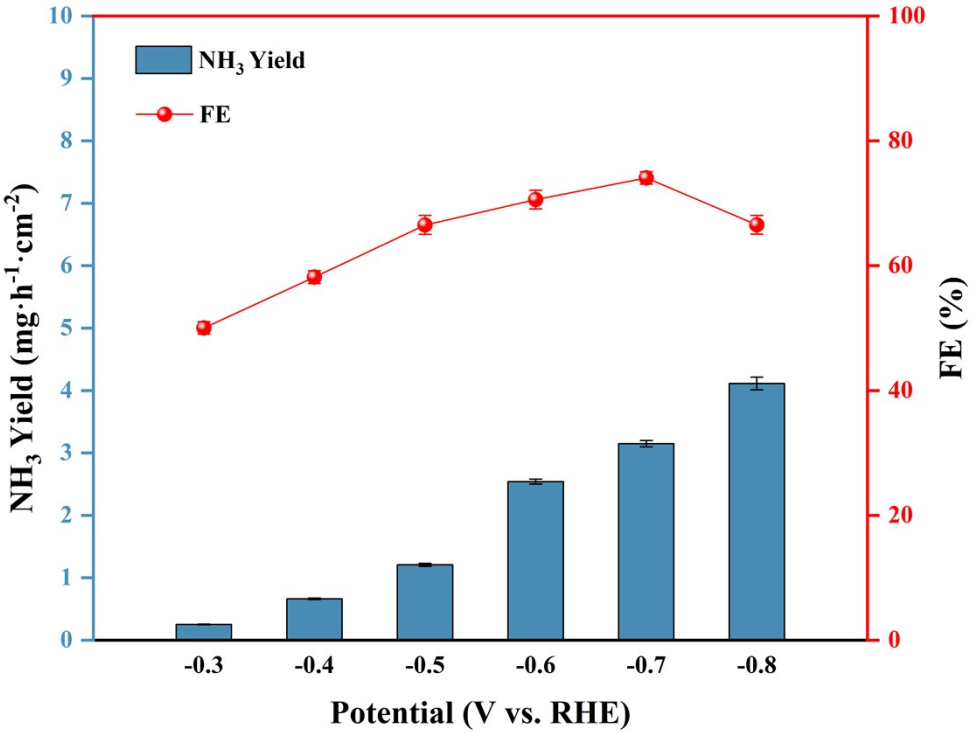

Fig. S18 NH_3 yield and FEs of Mo_7/Cu@CF.

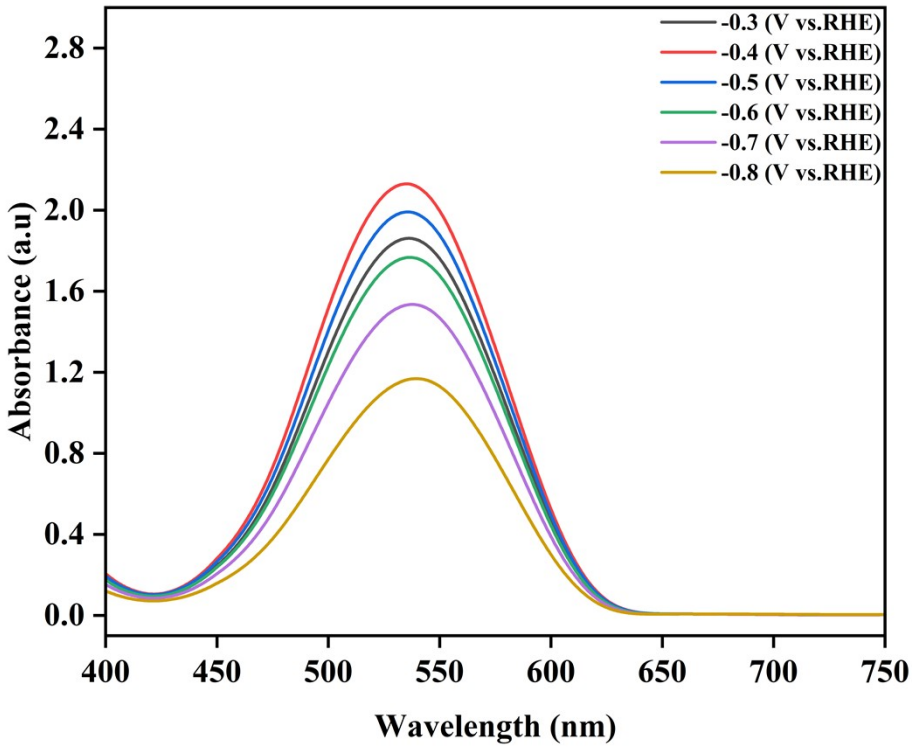

Fig. S19 UV–vis absorption NO_2^- spectra of $Mo_7/Cu_{2+1}O/Cu@CF$.

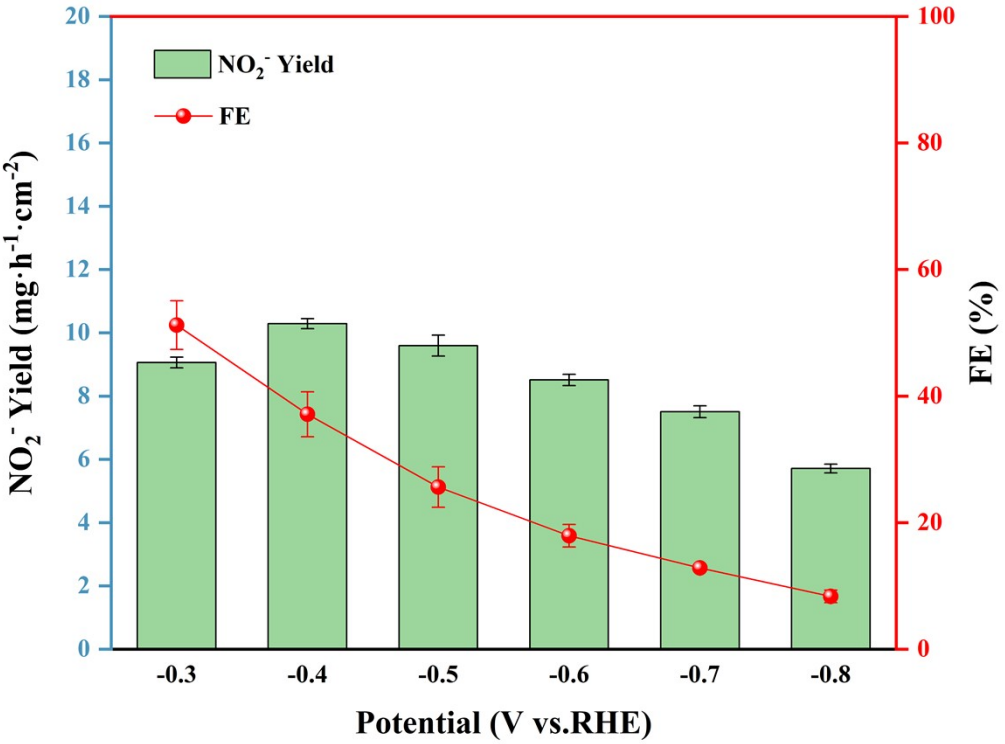

Fig. S20 NO_2^- yield and FEs of $Mo_7/Cu_{2+1}O/Cu@CF$.

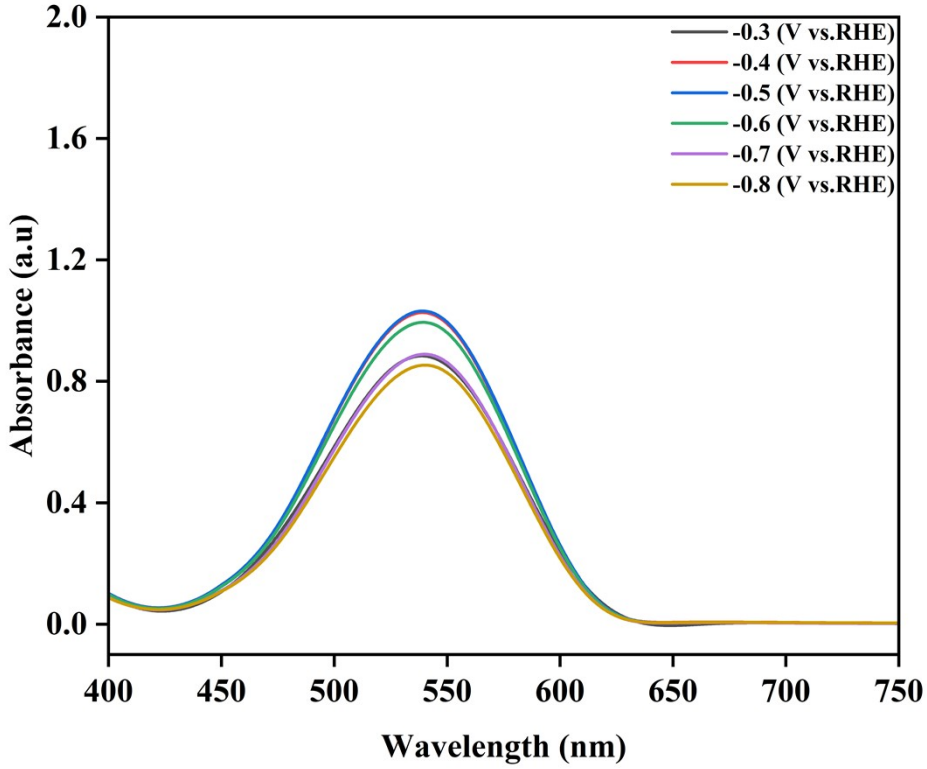

Fig. S21 UV–vis absorption NO_2^- spectra of $Cu_{2+1}O$/Cu@CF.

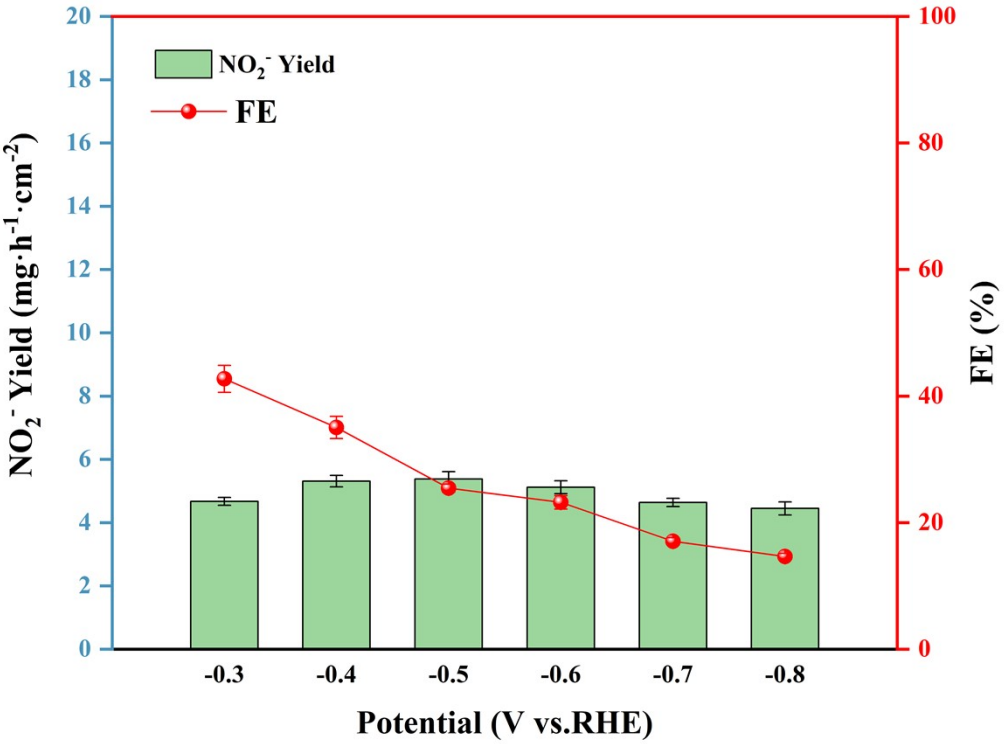

Fig. S22 NO_2^- yield and FEs of $Cu_{2+1}O$/Cu@CF.

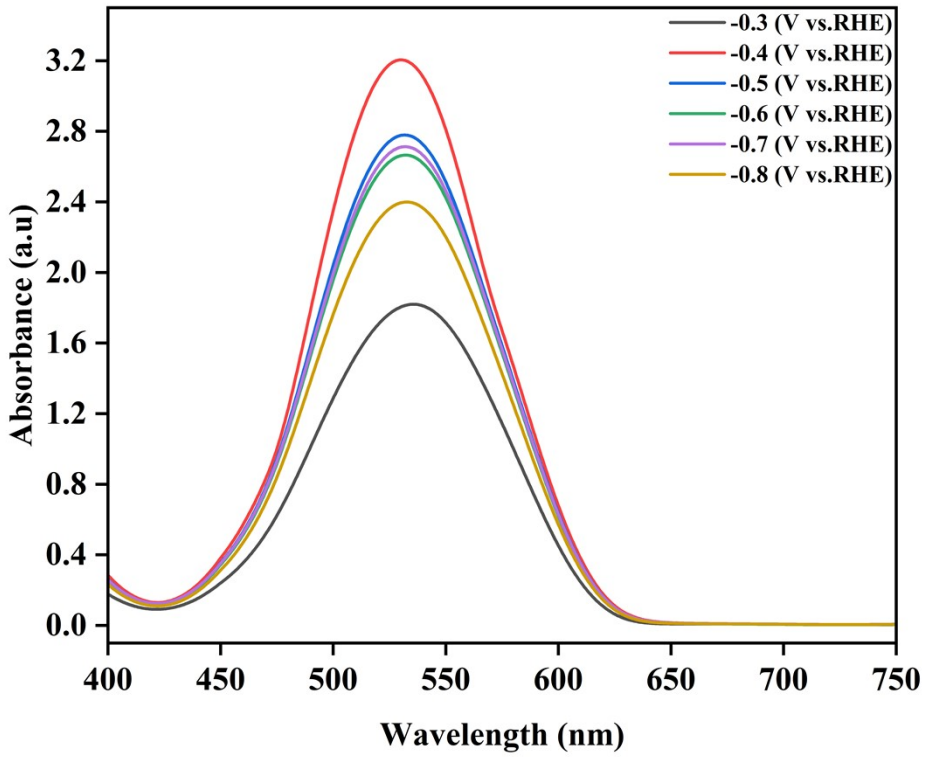

Fig. S23 UV–vis absorption NO_2^- spectra of Mo_7/Cu@CF.

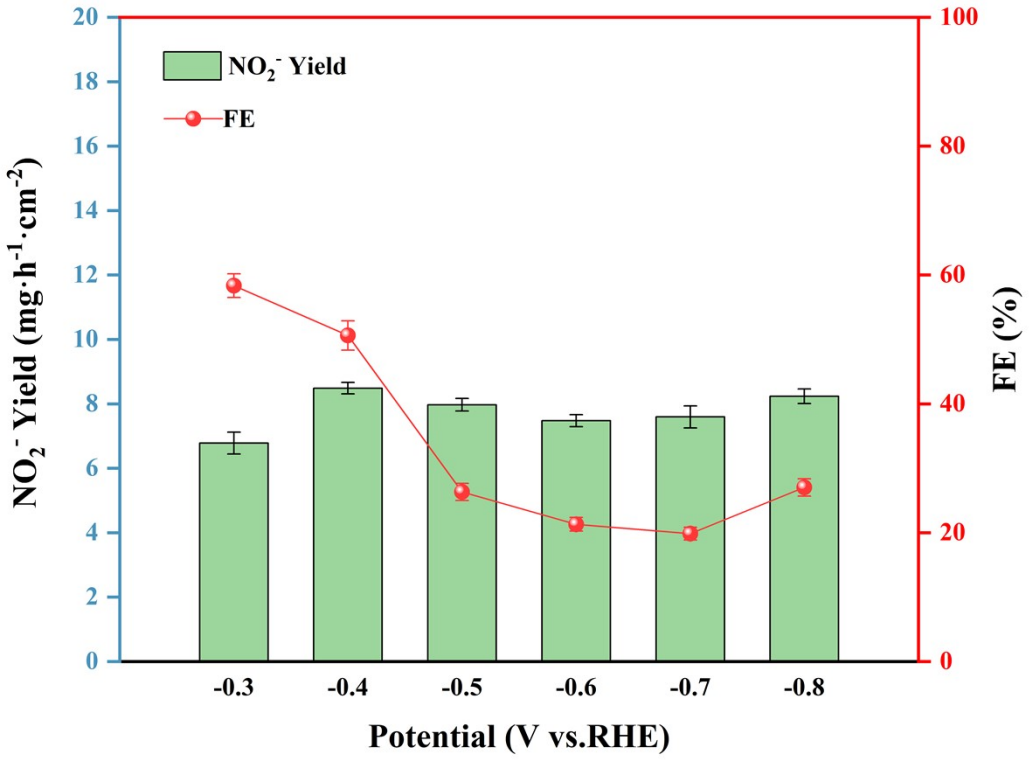

Fig. S24 NO_2^- yield and FEs of Mo_7/Cu@CF.

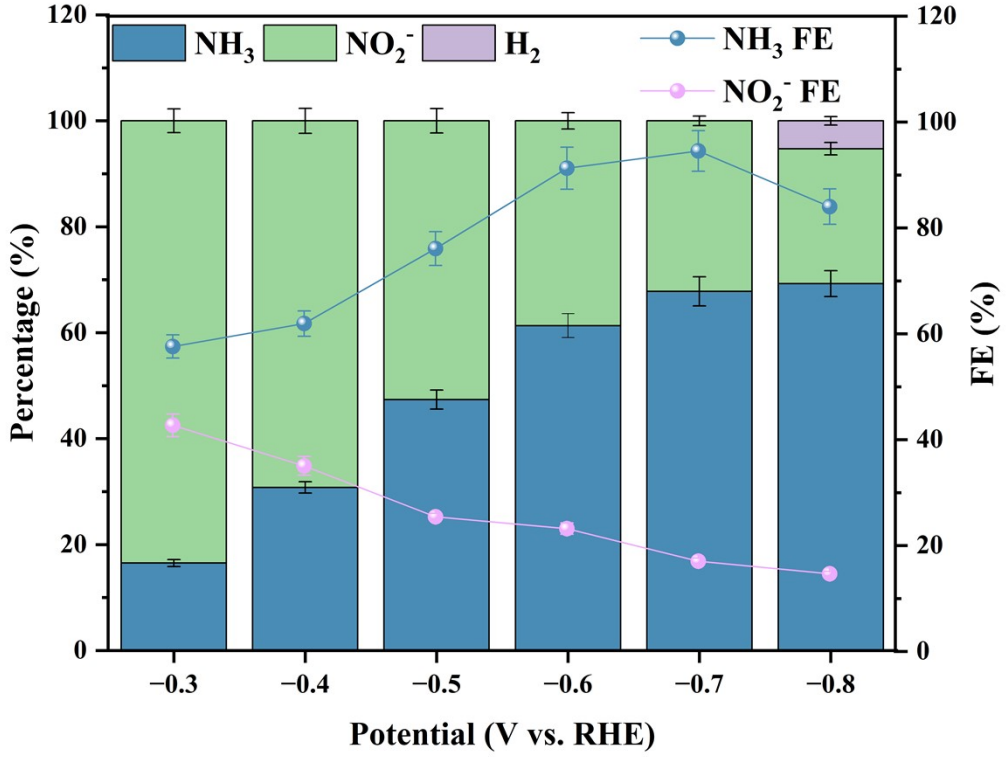

Fig. S25 At different potentials, $Cu_{2+1}O$/Cu@CF produces the proportion of NH_3, NO_2^- and H_2, FE of NH_3 and FE of NO_2^-.

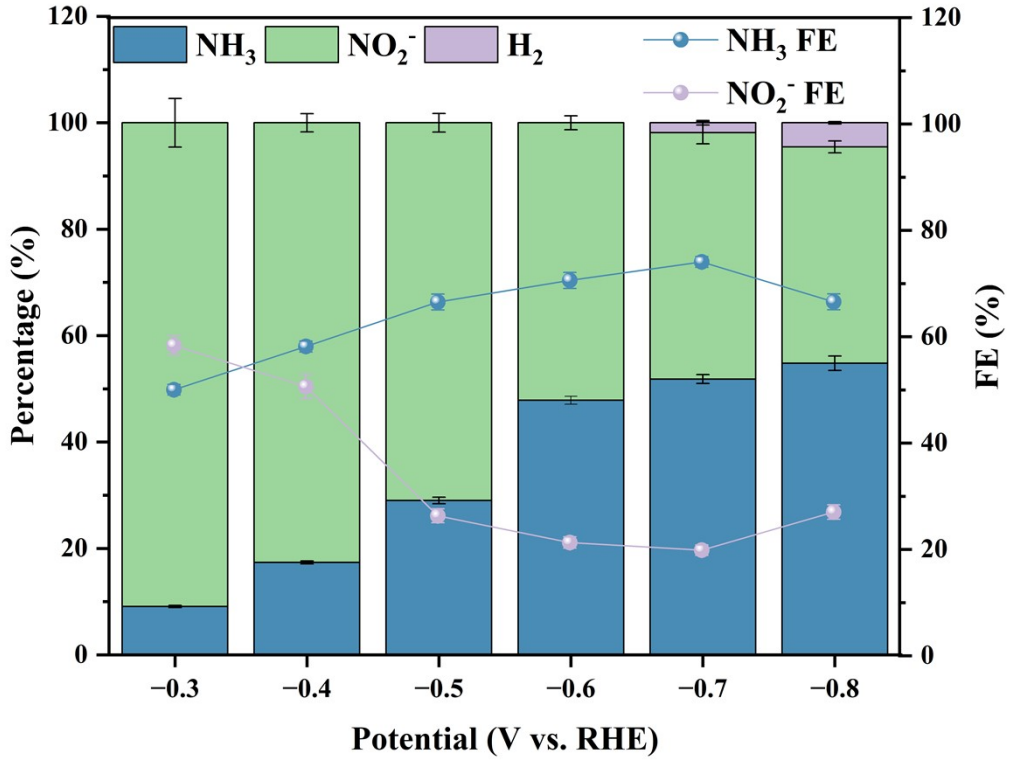

Fig. S26 At different potentials, Mo_7/Cu@CF produces the proportion of NH_3, NO_2^- and H_2, FE of NH_3 and FE of NO_2^-.

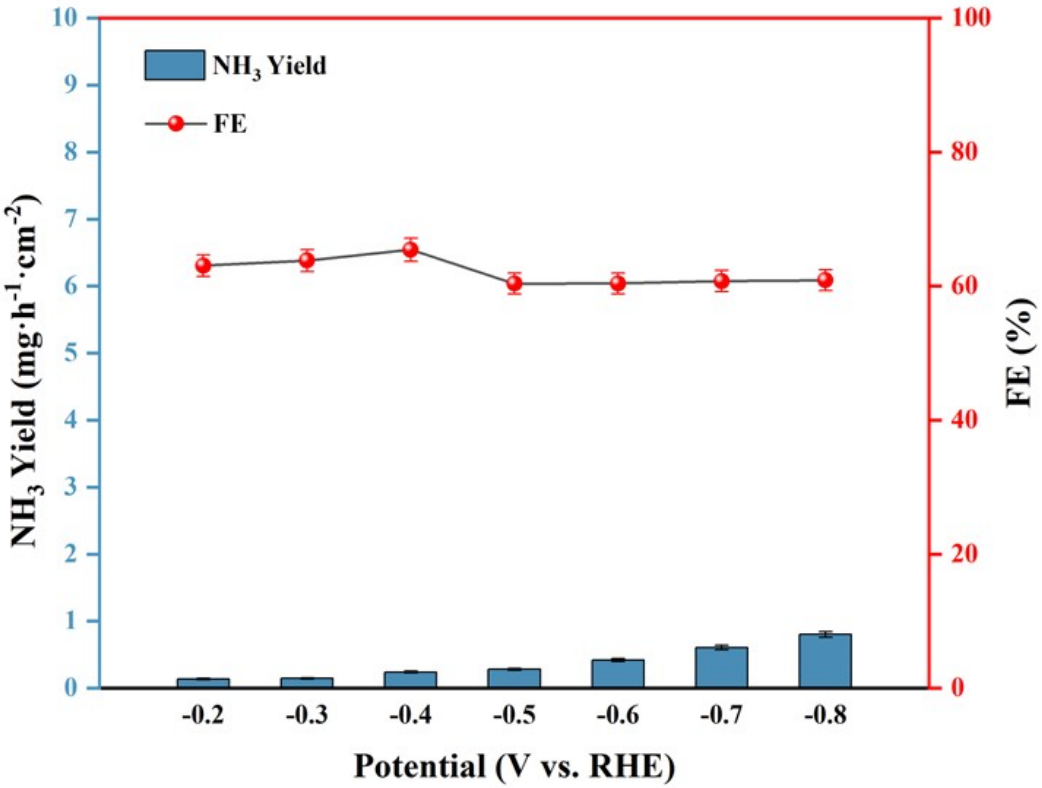

Fig. S27 NH_3 yield and FEs of bare copper foam.

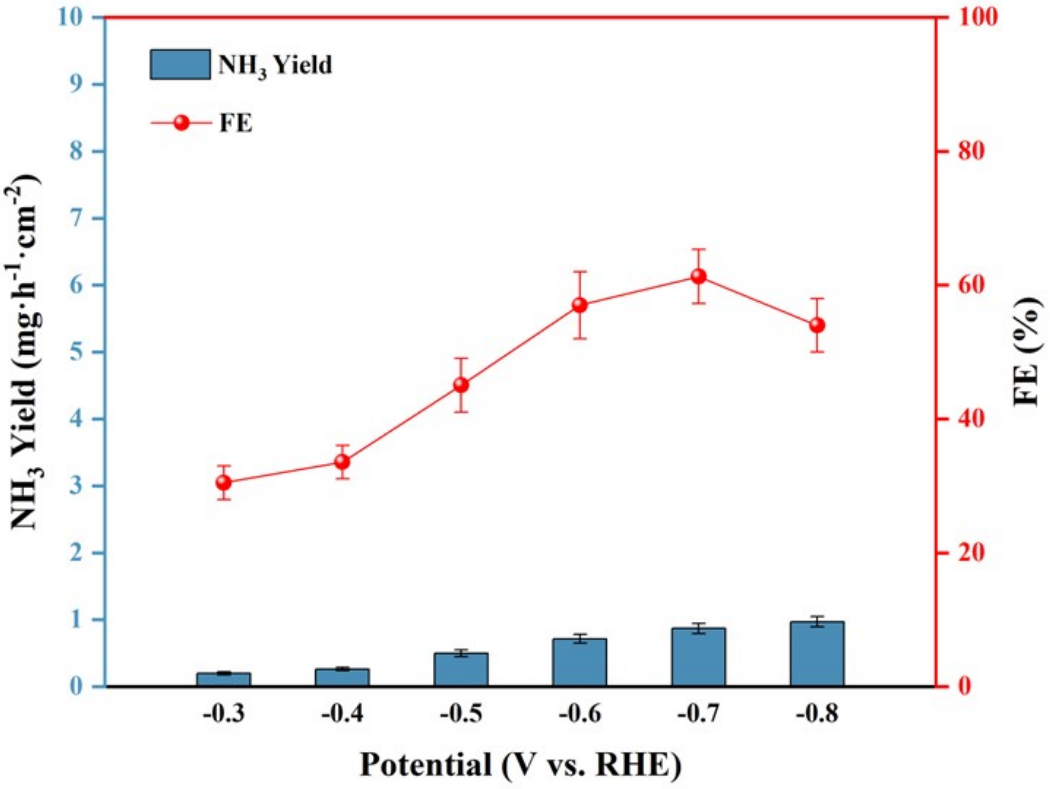

Fig. S28 NH_3 yield and FEs of Mo_7-TBAB.

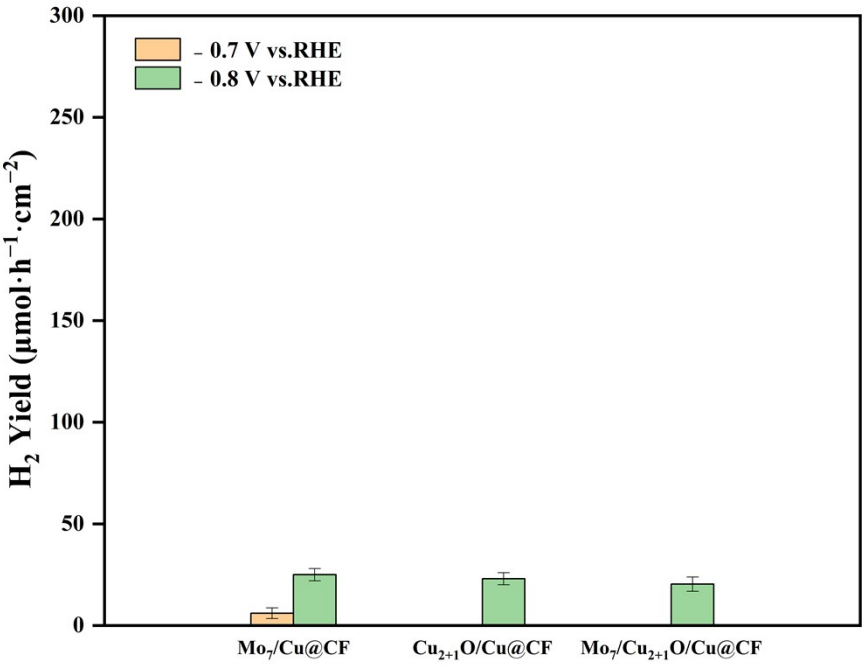

Fig.S29 H_2 yield of Mo_7/Cu@CF , $Cu_{2+1}O$/Cu@CF and $Mo_7/Cu_{2+1}O$/Cu@CF.

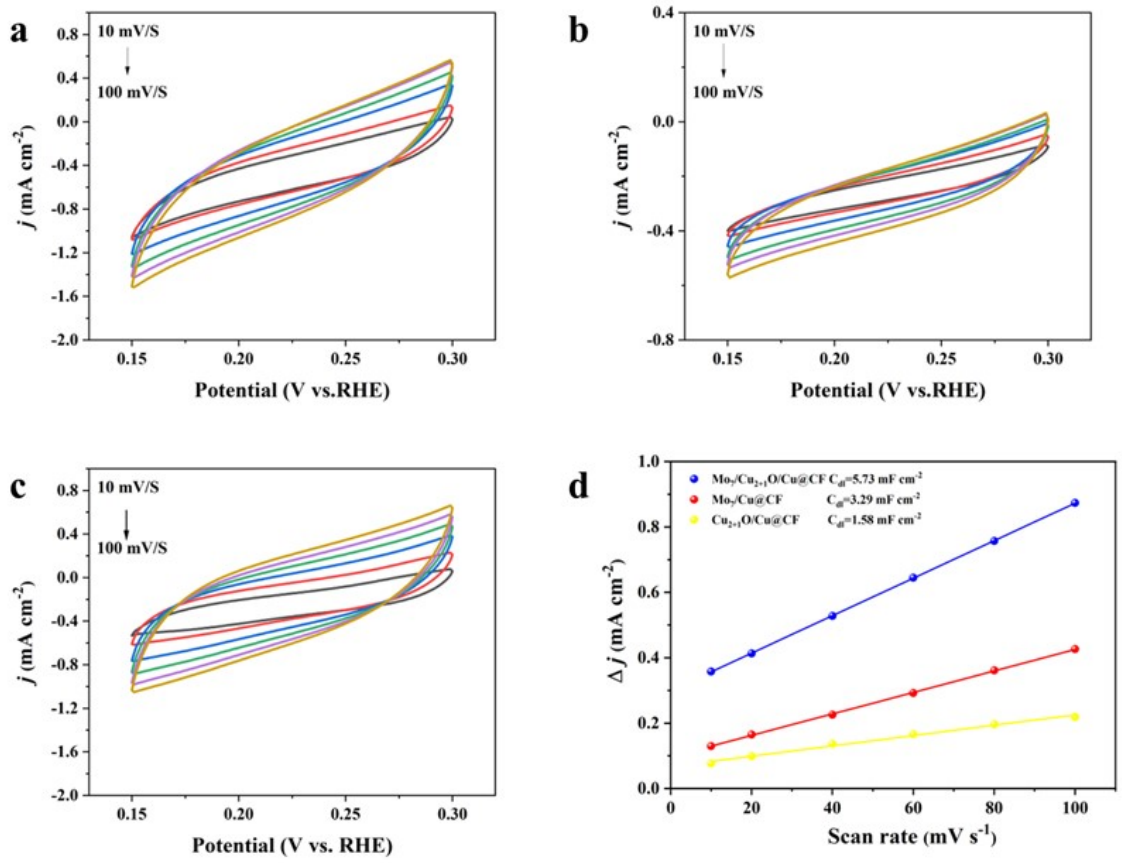

Fig. S30 The cyclic voltammetry curves of a) $Mo_7/Cu_{2+1}O/Cu@CF$, b) $Cu_{2+1}O/Cu@CF$, c) $Mo_7/Cu@CF$; e) the current density-scan rate plot of $Mo_7/Cu_{2+1}O/Cu@CF$, $Cu_{2+1}O/Cu@CF$ and $Mo_7/Cu@CF$.

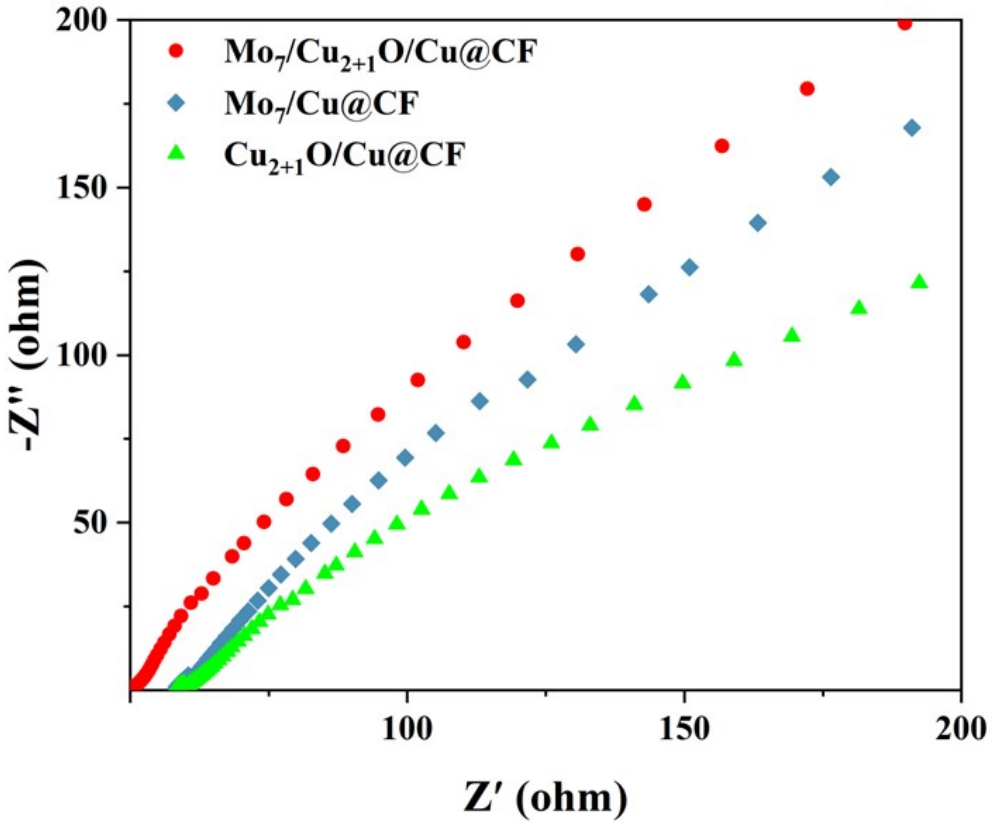

Fig. S31 Electrochemical impedance spectra of $Mo_7/Cu_{2+1}O/Cu@CF$, $Cu_{2+1}O/Cu@CF$ and $Mo_7/Cu@CF$.

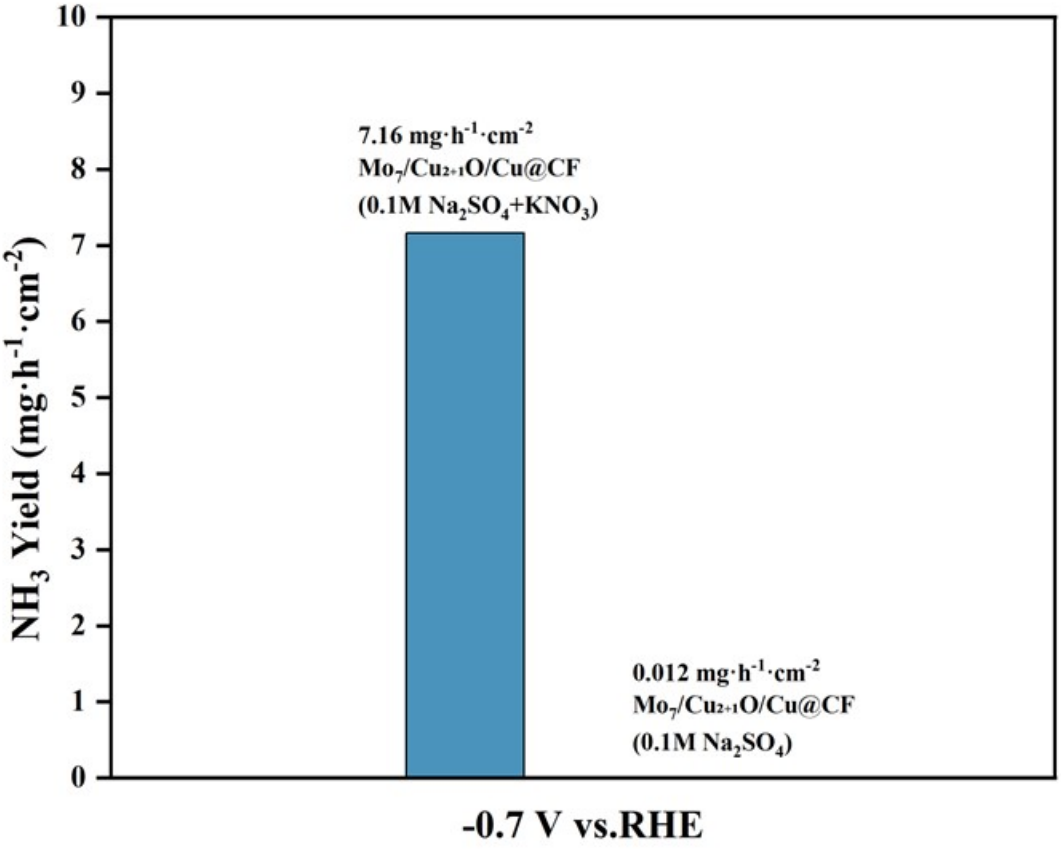

Fig. S32 The ammonia production rates of $Mo_7/Cu_{2+1}O/Cu@CF$ in 0.1 M Na_2SO_4 solution, with and without nitrate, were measured.

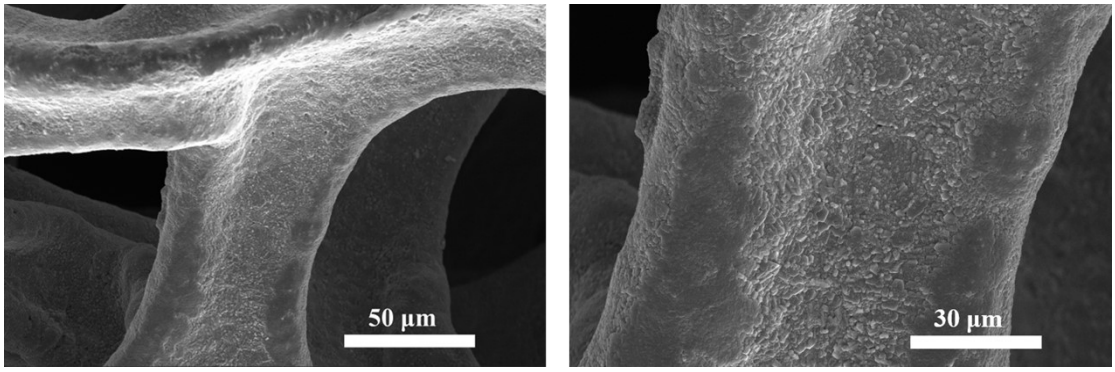

Fig. S33 SEM images of $Mo_7/Cu_{2+1}O/Cu@CF$ after 10 h continuous reaction.

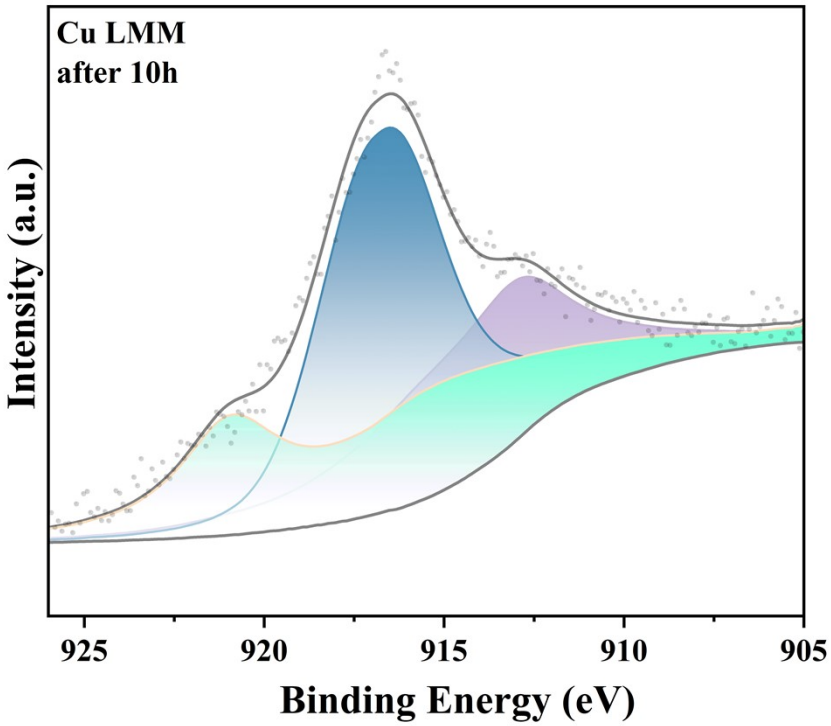

Fig. S34 Cu LMM XAES spectra of $Mo_7/Cu_{2+1}O/Cu@CF$ after 10 h continuous reaction.

Table S1. Summary of representative published work on electrocatalytic nitrate reduction.

Catalyst	Electrolyte	yield rate (NH_3)	FE (%)	Ref.
$Mo_7/Cu_{2+1}O/Cu@CF$	0.1 M Na_2SO_4 + 0.1 M KNO_3	7.16 $mg·h^{-1}·cm^{-2}$	95.7	This work
$Cu_{2+1}O/Cu@CF$	0.1 M Na_2SO_4 + 0.1 M KNO_3	3.64 $mg·h^{-1}·cm^{-2}$	89.2	This work
Mo_7/ Cu@CF	0.1 M Na_2SO_4 + 0.1 M KNO_3	3.14 $mg·h^{-1}·cm^{-2}$	74.2	This work
RuNi–MOFs	0.1 M Na_2SO_4 + 50 $mg·L^{-1}$ $NaNO_3$	1713 $\mu g·h^{-1}·cm^{-2}$	96.6	1
VCu–Au1Cu SAAs	0.1 M KOH + 7.14mM $NaKNO_3$	555 $\mu g·h^{-1}·cm^{-2}$	98.7	2
Cu nanosheet	0.1 M KOH + 10 mM KNO_3	78.02 $\mu g·h^{-1}·cm^{-2}$	99.7	3
RuCu	1 M KOH + 0.1 M KNO_3	6460 $\mu g·cm^{-2}·h^{-1}$	98	4
$Ru_{15}Co_{85}$	0.1 M KNO_3 + 0.1 M KOH	3.21 ± 0.17 $mol·g_{cat}^{-1}·h^{-1}$	96.78	5
FeCoNiAlTi	0.2 M K_2SO_4 + 50 mM KNO_3	520 $\mu g·h^{-1}·cm^{-2}$	95.23	6

Cu–incorporated	0.1 mM PBS + 36 mM NO_3^-	436 μg·h^{-1}·cm^{-2}	85.9	7
Au nanocrystals–Co_3O_4	1 M KOH + 0.5 M KNO_3	27.86 μg·h^{-1}·cm^{-2}	83.1	8
Ru-Tta-Dfp	1 M KOH + 100 mM KNO_3	1.16 mg·h^{-1}·cm^{-2}	93.3	9
Cu@Th-BPYDC	1 M KOH + 100 mM KNO_3	3.83 mg·h^{-1}·cm^{-2}	92.5	10

1. J. Z. Qin, K. Wu, L. Z. Chen, X. T. Wang, Q. L. Zhao, B. J. Liu and Z. F. Ye, *J. Mater. Chem. A*, 2022, **10**, 3963-3969.
2. Y. Z. Zhang, X. Chen, W. L. Wang, L. F. Yin and J. C. Crittenden, *Appl. Catal. B-Environ. Energy*, 2022, **310**, 11.
3. X. B. Fu, X. G. Zhao, X. B. Hu, K. He, Y. N. Yu, T. Li, Q. Tu, X. Qian, Q. Yue, M. R. Wasielewski and Y. J. Kang, *Appl. Mater. Today*, 2020, **19**, 6.
4. W. S. Gao, K. F. Xie, J. Xie, X. M. Wang, H. Zhang, S. Q. Chen, H. Wang, Z. L. Li and C. Li, *Adv. Mater.*, 2023, **35**, 9.
5. S. H. Han, H. J. Li, T. L. Li, F. P. Chen, R. Yang, Y. F. Yu and B. Zhang, *Nat. Catal.*, 2023, **6**, 402-414.
6. R. Zhang, Y. Q. Zhang, B. Xiao, S. C. Zhang, Y. B. Wang, H. L. Cui, C. Li, Y. Hou, Y. Guo, T. Yang, J. Fan and C. Y. Zhi, *Angew. Chem.-Int. Edit.*, 2024, **63**, 7.
7. G. F. Chen, Y. F. Yuan, H. F. Jiang, S. Y. Ren, L. X. Ding, L. Ma, T. P. Wu, J. Lu and H. H. Wang, *Nat. Energy*, 2020, **5**, 605-613.
8. M. L. Zhang, K. P. Song, C. Liu, Z. D. Zhang, W. Q. He, H. Huang and J. L. Liu, *J. Colloid Interface Sci.*, 2023, **650**, 193-202.
9. A. Chaturvedi, S. Gaber, S. Kaur, K. C. Ranjeesh, T. C. Nagaiah and D. Shetty, *ACS Energy Lett.*, 2024, **9**, 2484-2491.
10. Z. Gao, Y. L. Lai, Y. Tao, L. H. Xiao, L. X. Zhang and F. Luo, *ACS Central Sci.*, 2021, **7**, 1066-1072.